Materials Chemistry and Physics 304 (2023) 127867

Contents lists available at ScienceDirect

Materials Chemistry and Physics

journal homepage: www.elsevier.com/locate/matchemphys

Mechanical properties and biocompatibility of various cobalt chromium dental alloys

Anca Fratila [a], Cristina Jimenez-Marcos [b], Julia Claudia Mirza-Rosca [b,c,*], Adriana Saceleanu [a]

[a] "Lucian Blaga" University of Sibiu, Medicine Faculty, 550024, Sibiu, Romania
[b] Las Palmas de Gran Canaria University, Department of Mechanical Engineering, Tafira, 35017, Spain
[c] Transilvania University of Brasov, Materials Engineering, and Welding Department, 500036, Brasov, Romania

HIGHLIGHTS

- Dental alloys undergo spontaneous passivation due to a passive film on their surface.
- The passive potential range is large and the samples showed a good pitting corrosion resistance.
- The thickness of the passive film increases with the potential, with a capacitive response over a wide frequency range.
- Young's modulus was lowest for tungsten-rich sample with 3 points bending test.

GRAPHICAL ABSTRACT

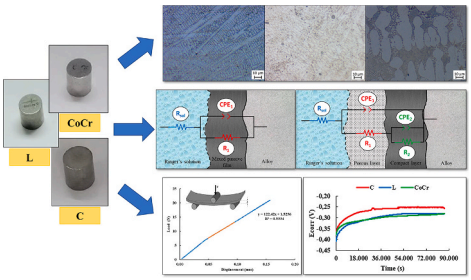

ARTICLE INFO

Keywords:
Dental alloys
Co–Cr
Microstructure
Corrosion
Three-point bending test

ABSTRACT

Cobalt-based metal alloys are often used in dentistry for prosthetic restorations because of their considerable wear and corrosion resistance. For this reason, the effect on the human body of three Co–Cr based alloys, named "Co–Cr", "C" and "L", differing in their concentrations, for subsequent use as dental materials, has been studied and compared. Metallographic observations of the microstructure, electrochemical and three-point bending tests were performed. The metallographic investigations showed similar dendritic microstructure of the Co–Cr and L dental alloys, as well similar porosities and defects. From the corrosion and pitting potential tests, it was found that the samples show surface passivation, reaching closed corrosion potential values from −0.280 V vs SCE to −0.250 V vs SCE. The Pitting Resistance Equivalent Number (PREN) values are above 38 for all the samples, which means that the studied alloys have a high resistance to pitting corrosion. Likewise, when applying the Electrochemical Impedance Spectroscopy technique, a slightly higher corrosion resistance was observed for sample L, since corrosion resistance tends to increase as the applied potential is more positive and as the impedance and phase angle values are higher. Moreover, in the three-point bending test, the alloy C presents the lowest values of the elastic modulus of 134 ± 13 GPa. The analyzed Co–Cr alloys are recommended for the efficient treatment of patients with dental prostheses that have metal frameworks, as shown by all of the obtained results.

* Corresponding author. Las Palmas de Gran Canaria University, Department of Mechanical Engineering, Tafira, 35017, Spain.
E-mail address: julia.mirza@ulpgc.es (J.C. Mirza-Rosca).

https://doi.org/10.1016/j.matchemphys.2023.127867
Received 24 January 2023; Received in revised form 21 April 2023; Accepted 30 April 2023
Available online 5 May 2023

1. Introduction

Metallic biomaterials are of great importance in biomedical devices and components for joint replacements, orthopedic fixations, dental implants and stents due to their good combination of tensile strength, fatigue strength and fracture toughness. Yet, the successful and regular use of these biomaterials has encountered problems related to the long-term maintenance of the implants or even biocompatibility issues [1–8].

In general, these materials are divided into four broad classes according to their main alloying elements: Stainless steel, cobalt, titanium, with these three routinely used as implants, and finally some others such as Mg, Ni, Ti and tantalum alloys that are accepted by the Food and Drug Administration and are in clinical trials [7,9–12].

In the field of dental prosthetics, metallic biomaterials have been widely used since the early 19th century, when precious metals such as gold, silver or platinum were used until they were later replaced by Ni- and Co-alloys due to their high cost [13,14].

Dental implants are nowadays a viable treatment solution for the oral rehabilitation of partially or completely edentulous patients, although cost-effective and safe surgical and prosthetic protocols in this area are still under development [15,16]. Consequently, metallic materials used in dentistry must meet several requirements for their properties, such as good biocompatibility, non-toxicity, safety, stability, good wear resistance and hardness, to name a few. These requirements include biocompatibility and thus corrosion resistance, as metals and their alloys in contact with oral tissues can cause undesirable tissue reactions and hypersensitivity reactions due to the release of elements into the oral cavity while the corrosion process is taking place [1,9,17,18]. The corrosion properties of these materials depend on various factors such as the composition of the alloy, potential values, surface roughness, stress, oxidation degree, pH, media temperature, solution mixing rate and the presence of inhibitors [19,20].

In dentistry, metal ions have complicated side-effects on the human body and, function of exposure time, concentration and route of administration, four major different biological responses can be identified: (i) essential or trace elements (Co, Cu, Fe, Zn, Mn, Ni) present in very low concentrations; (ii) possible toxic reactions in humans due to high concentrations of elements such as, Co, Ni, Pb, etc.; (iii) the allergenic potency of elements such as Cr, Ni and Co, which are well known sensitizers, and finally (iv) carcinogens for which there is no clinical and/or statistical evidence of dental alloys causing cancer [21].

Porcelain-fused-to-metal (PFM) crowns are frequently used to repair severely chipped teeth and protect the remaining tooth structure [22]. Porcelain-fused-to-metal fixed dental prostheses (PFM-FDP) also merge the aesthetics of porcelain with the strength of metal and have been used as the standard and predominant aesthetic choice for dental restoration due to their good clinical performance with low failure rates. Furthermore, its success is highly dependent on the physical properties of the employed material [23,24]. This type of framework can be made with different types of dental casting alloys thanks to the improvement of materials and techniques, always taking into account the biocompatibility of the materials used [24].

Nickel- and cobalt-based alloys are, considering cost and strength among the most used alloys for the construction of fixed and removable dentures, [25,26]. With increasing health awareness, nickel-based dental alloy materials, mainly used for bridges and crowns, has aroused concerns among patients and dentists due to nickel metal ions that are released and have immunogenic, toxic, mutagenic and chemotactic effects [11,24,27,28]. In many countries, such as the United States of America, it has therefore been decided to replace these alloys with cobalt-chromium alloys for denture fixation [29–31].

Cobalt-based alloys, mainly Co–Cr, are characterized by high creep, corrosion, wear and temperature resistance, non-magnetic properties and hardness [6,29,32–36]. In addition, these alloys have been shown to be cytocompatible and can therefore perform their function without adverse effects on the patient [29,36–38]. For example, the addition of chromium in this type of alloy provides hardness, stability and resistance and can improve the corrosion behavior of the alloy when its concentration is between 16 and 20 wt%, forming a thin passive protective film under oxidizing conditions [10,39–45]. When using these alloys, there is a very small percentage of patients with corresponding allergic reactions, but the metal ions can be released and cause reactions in the human organism [46,47].

The addition of Mo or other elements like tungsten or Cu in these alloys reduces the corrosion rate under conditions where these alloys are not covered by the passive layer or where the passive layer is breached [40,41,48].

In this study, three Co–Cr-based dental alloys, availables on spanish dental material market, were investigated and compared. Corrosion potential, pitting potential, electrochemical impedance spectroscopy and three-point bending tests were used to investigate their corrosion and mechanical behavior in Ringer's solution and to confirm their feasibility and biocompatibility for further use as dental materials, mainly for prosthetics. As these metal alloys encounter physiological fluids during use, corrosion products could cause local and systemic reactions in the immune system. As a result, it's critical to comprehend the corrosion resistance of these alloys in physiological fluids as well as their modulus of elasticity in these conditions.

2. Materials and methods

2.1. Material preparation

Three samples in the form of cylindrical bars of a CoCr alloy with the designations "CoCr", "C" and "L", which differ in their composition, were used for the study.

The manufacturer of the CoCr sample is DeguDent, a German company that develops and produces high-quality materials, instruments and equipment for medical laboratories worldwide. The C and L samples come from the US company Dentsply Sirona, a manufacturer of medical equipment and consumables.

The composition of the three studied samples provided by the manufacturers is shown in Table 1.

As a preliminary step to the metallographic, electrochemical and bending tests, the samples were embedded in a mixture of epoxy resin and a catalyst in a ratio of 4:1 into a mould, and dried for 24 h. The cylindrical bars were cut into plates with a thickness of 5 mm using a Buehler IsoMet 4000 linear precision saw (Chicago, IL, USA) fallowed by grinding and polishing using a Struers TegraPol-11 polishing machine (Copenhagen, Denmark) at a speed of 300 rpm and a force of 20 N. For grinding, SiC abrasive papers were used with different grit sizes starting with P400 and finishing with P2500 grit size. Finally, 0.1 μm alumina suspension on a polishing cloth was used to achieve a mirror-like polish. After polishing, the samples were immersed in a heated J.P. Selecta "Ultrasons- HD" ultrasonic unit (Abrera, Barcelona, Spain) for 5 min to eliminate any trace of contamination. The sample preparation protocol was in accordance with ASTM E3-11(2017) for metallographic testing. For the mechanical tests, the cylindrical bars were cut vertically into plates of about 2 mm thickness by using the precision saw (see Fig. 1).

2.2. Microstructure

Metallography allows to study the microstructure and compounds that constitute a metallic material as well as the impurities or mechanical defects that may be present in such materials [28].

To investigate the microstructure of the samples, micrographs of the surfaces of each sample were recorded using a Axio Vert.A1 MAT ZEISS optical microscope (Jena, Germany) at different magnifications. Each sample was immersed in a reagent of 10 ml nitric acid, 30 ml hydrochloric acid and 20 ml glycerine, at intervals of 1–3 min depending on the sample, and the attacked surface was afterwards investigated.

Table 1
Composition (wt.%) of the studied alloys.

Alloy	Elements %											
	Co	Cr	Mo	W	Nb	V	Si	Mn	Fe	C	N	Ni
CoCr	64.8	28.0	5.0	–	–	–	<0.1	<0.1	–	<0.1	<0.1	<0.1
L	62.5	30.5	5.0	–	–	–	1.0	0.4	–	0.3	0.3	–
C	59.4	24.5	1.0	10.0	2.0	2.0	1.0	–	0.1	–	–	–

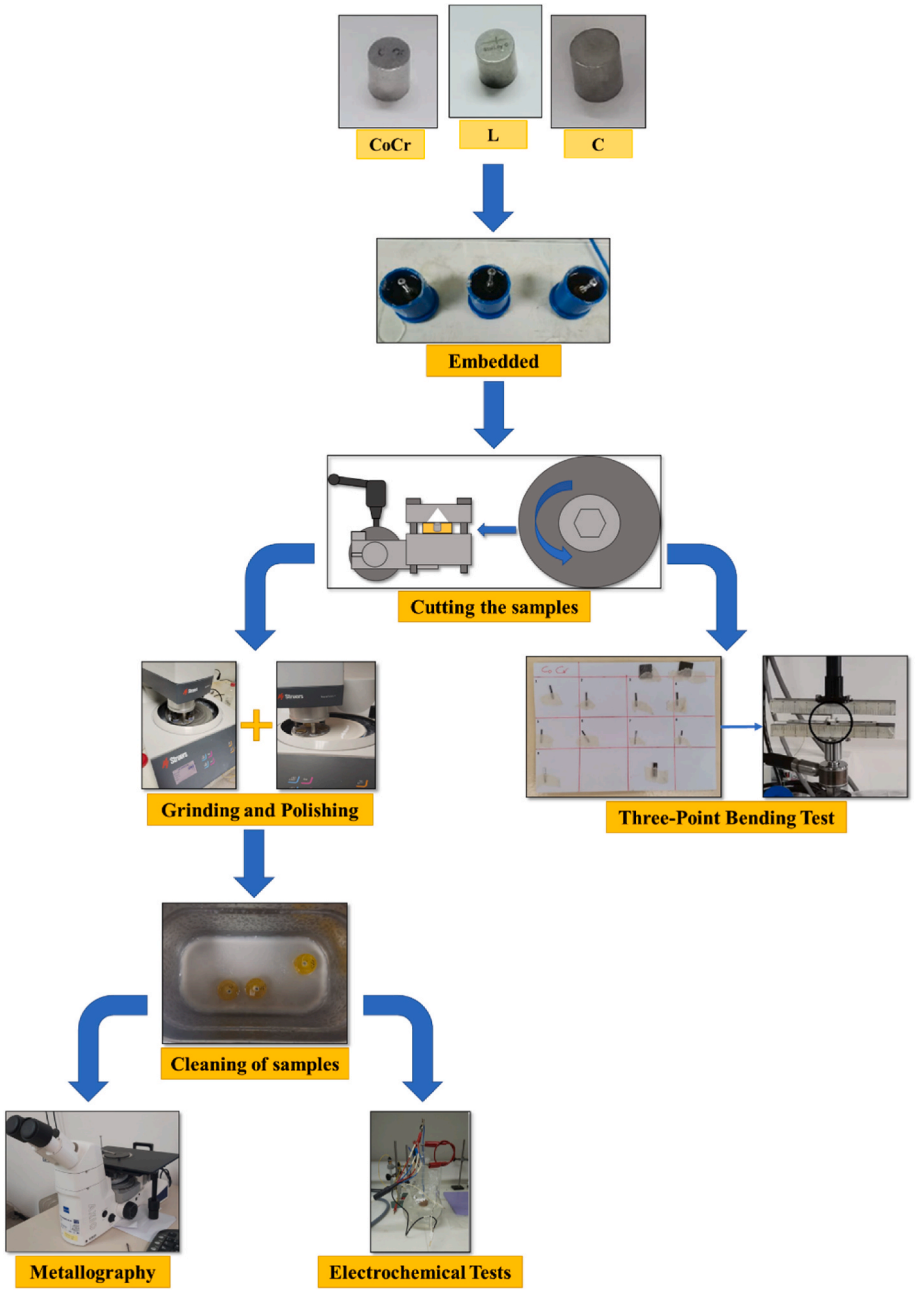

Fig. 1. Schematic representation of the samples' preparation.

2.3. Electrochemical tests

The electrochemical tests consist of imersing a sample into an electrolite within an electrochemical cell, which therefore has three electrodes: a reference electrode (saturated calomel), a counter electrode (platinum electrode) and a working electrode (the investigated sample). In order to perform the tests, the area of each investigated sample was calculated using ImajeJ software. The Ringer Grifols solution (Grifols Laboratories, Barcelona, Spain) had the following contents in mmol/L: Na^+ 129.9; K^+ 5.4; Ca^{2+} 1.8; Cl^- 111.7; and $C_3H_5O_3$ 27.2.

To investigate the corrosion bahviour of the alloys, three techniques were employed using a potentiostat-galvanostat BioLogic Essential SP-150 (Seyssinet-Pariset, France) in the following order: (i) corrosion potential, (ii) electrochemical impedance spectroscopy and (iii) pitting

potential.

2.3.1. Corrosion potential

The 24-h corrosion potential of each sample was measured using the "Ecorr vs. Time" technique available in the EC-Lab software. The potential values used were ±10 V with the potential recorded at every 300 s and varying the time at every 100 mV. The obtained data was processed and plotted as a graph of potential versus time.

2.3.2. Pitting potential

The pitting potential was measured in the electrochemical electrolysis cell using the "Depassivation potential" technique available in the EC-Lab software. The maximum and minimum potential values were ±10 V, with the potential scanning presenting a 60 mV/mn time-variation relationship from −0.4 to 1.0 V versus open circuit potential (OCP). Data recording was performed till 1.0 mA. The data obtained with this technique were plotted in a graph current versus potential.

2.3.3. Electrochemical impedance spectroscopy

The EIS procedure was performed for 5 min. Furthermore, this procedure was applied 3 times for each sample at 3 different potential values from −0.4 to 0.4 V vs. OCP in Ringer's solution by selecting "Potentio Electrochemical Impedance Spectroscopy" in the EC-Lab software, with maximum and minimum potential values of ±10 V. The data obtained was processed and plotted using Bode and Nyquist diagrams and based on the results the equivalent circuits was determined as well.

2.4. Three-point bending test

The three-point bending test was performed using the Bose ElectroForce® 3100 testing machine, in accordance with ISO 7438:2020 Metallic materials standard. The machine can withstand an applied force of up to 20 N. In this case, each rectangular specimen was approximately 11 mm long and the distance between the supports was 7.93 mm. The load was applied verically with a linear velocity of 3 mm/s applied to the central part of each sample until it exceeded the elastic limit of the material or broke to obtain its deformation.

The obtained values were plotted in a graph applied force versus displacement and based on the obtained linear slopes the modulus of elasticity was to calculate.

3. Results and discussions

3.1. Microstructural investigation

The surfaces of the three investigated samples after etching are shown in Fig. 2 at x50 and ×100 magnification. After the electrochemical etching, a dendritic structure of the CoCr-based samples can be seen. The microstructure of the Co–Cr–Mo and L alloys is dendritic which is typical for cast materials. Compared to the literature the microstructure consists of a Co–Cr solid solution found in the matrix and a mixture of $M_{23}C_6$ carbides with austenite in the dendritic areas [49].

For the C sample, the microstructure consists of typical α-ffc phase encountered in the dendritic areas, colonies of interlayed α-ffc phase and M23C6 carbides which resembles with the perlitic structure, alongside with σ phase precipitates. The results are in accordance with the findings of Giacchi et al. when studding Co–Cr–Mo alloys with W content [50]. In addition, its composition is slightly different from that of the other two samples, as it does contain less molybdenum and instead contains 10% of tungsten.

3.2. Electrochemical tests

3.2.1. Corrosion potential

The curves of the corrosion potential versus time were analyzed after 24 h testing time (see Fig. 3 and Table 2). In these conditions, the potential is named open circuit potential (OCP) and indicates the anticorrosive tendency of the sample. Based on the obtained data, the curves of the three samples present similar behavior with a suddenly increasing of potential, reaching values between −0.305 V and 0.339 V after 2 h of immersion, due to the passivation of the dental materials. So, for all the three alloys, after 2-h of immersion, there was no damage of the passive layer. In general, during the 24-h test, the potentials of the CoCr, L and C samples increased due to thickening of the passive film, reaching final

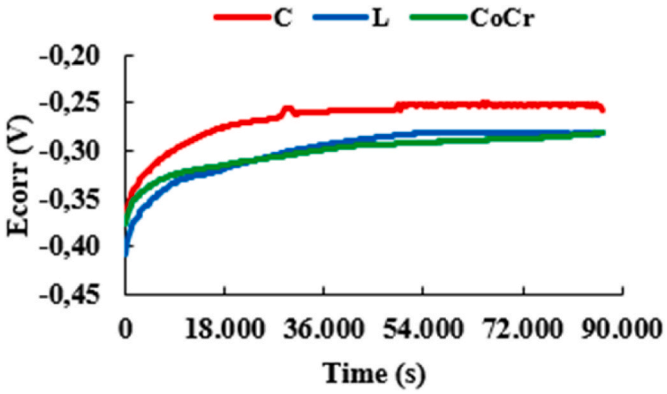

Fig. 3. Corrosion potential curves for CoCr, C and L alloys after 24 h immersion time.

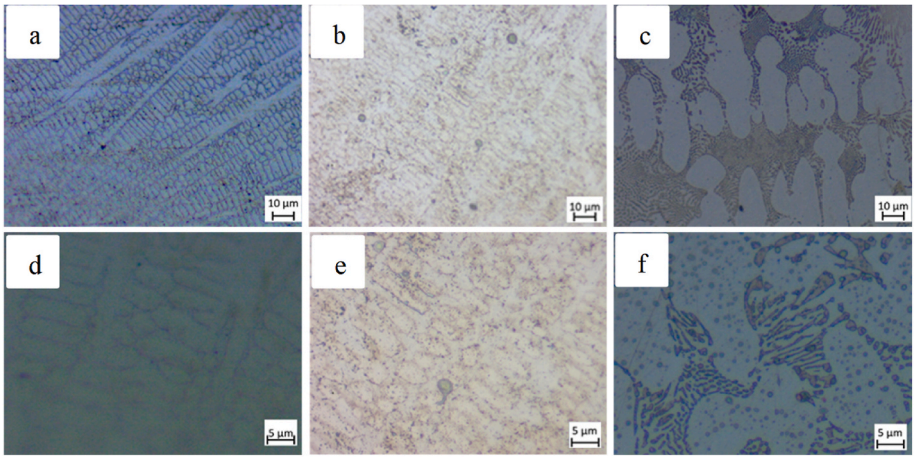

Fig. 2. Optical microstructure after reagent etching at ×50 magnification for CoCr (a), L (b) and C (c), and at ×100 magnification for CoCr (d), L (e) and C (f).

Table 2
Corrosion potential results: initial, after 2 h and 24 h, for the three samples immersed in Ringer Grifols electrolyte.

Alloy	Ecorr, mV vs SCE		
	Initial	After 2 h	After 24 h
CoCr	−0.376	−0.328	−0.280
L	−0.407	−0.339	−0.281
C	−0.372	−0.305	−0.250

values of −0.280 V, −0.281 V and −0.250 V, respectively; CoCr and L samples have almost the same corrosion potential value, while for the C sample the potential stabilised at a higher value. The increase and stabilisation trend of the corrosion potential of sample C may be due to the addition of 10% W, because tungsten can reduce the corrosion rate in the alloy [48]. The continuous shift of the potential towards noble values indicated, for all the investigated samples, that the passive layer was subjected to changes during the tests: it becomes more protective. Thus, immersion of the alloys in Ringer's solution for 24 h indicated that, from a qualitative aspect, the passivation tendency was high for all three samples.

During the immersion of the samples in open circuit conditions, different reactions will take place.

The metallic Cr has formed a passive oxide layer of Cr_2O_3, very protective, in accordance with reaction [51]:

$$2Cr + 3H_2O \rightarrow Cr_2O_3 + 6H^+ + 6e^- \quad (1)$$

The significant amount of cobalt favored the generation of an oxide, following the reaction:

$$Co + H_2O \rightarrow CoO + 2H^+ + 2e^- \quad (2)$$

This means that a mixed passive film of Cr_2O_3 and CoO was developed on the surface of the alloys; it improves the stability of the Cr_2O_3 film and mitigated the hydrolysis of Cr^{3+}, which occurred in the transpassive zone. At more possitive potentials, the oxidation of Cr^{3+} occurs to form soluble Cr^{6+}:

$$Cr_2O_3 + 5H_2O \rightarrow 2CrO_4^{2-} + 10H^+ + 6e^- \quad (3)$$

Among metals, tungsten has the highest melting point and one of the highest densities therefore is used to increasing the hardness, elasticity and tensile strength of the alloys [52]. Its oxidation occurs in 3 stages:

$$W + 2H_2O \rightarrow WO_2 + 4H^+ + 4e^- \quad (4)$$

$$2WO_2 + H_2O \rightarrow W_2O_5 + 2H^+ + 2e^- \quad (5)$$

$$2W_2O_5 + H_2O \rightarrow 2WO_3 + 2H^+ + 2e^- \quad (6)$$

and only the hexavalent oxide is stable in the presence of water at 25 °C.

Mo addition has many advantages when used as alloying element such as better melting point, prominent property at elevated temperatures, lower coefficient of thermal expansion and a very good thermal conductivity coefficient [53]. In the presence of neutral or slightly acid or alkaline solutions, it tends to cover itself with tetravalent dioxide MoO_2 according to reaction [51]:

$$Mo + 2H_2O \rightarrow MoO_2 + 4H^+ + 4e^- \quad (7)$$

3.2.2. Pitting potential

Potentiodynamic polarization measurements were made from −0.8 V to 0.8 V (SCE) to assess the pitting process (see Fig. 4).

With an anodic value of more than 500 mV, the resulting pitting potential of the three samples exhibited a good electrochemical stability (see Table 3).

During the imersion of the samples in Ringer's solution, surface passivation had the beneficial effect of reducing the corrosion current and shifting the breakdown potential to more anodic values.

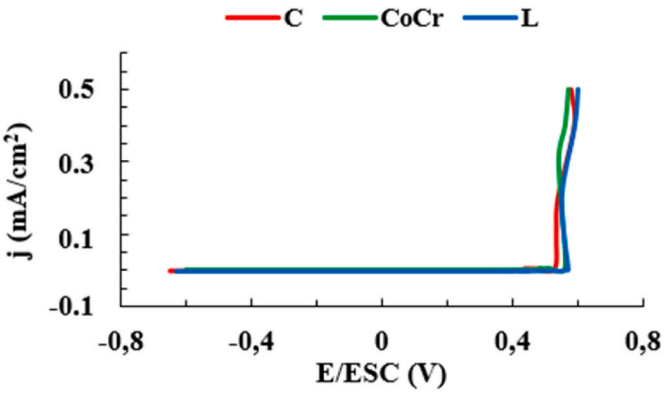

Fig. 4. Pitting potential curves for CoCr, C and L alloys.

Table 3
Voltage and current values at which pitting occurred.

Samples	(μA/cm^2)	(V)
CoCr	5.10	0.56
L	4.90	0.57
C	5.30	0.53

Thus, the three alloys displayed a broad passivation range and modest passivation currents between 4 and 5 μA/cm^2 under these circumstances.

A qualitative method for determining how susceptible corrosion-resistant metals are to pitting corrosion is the Pitting Resistance Equivalent Number (PREN). It is determined by taking into account an alloy's concentration of chromium (Cr), molybdenum (Mo), tungsten (W), and nitrogen (N). The material was more resistant to localized pitting corrosion because of its higher PREN value [54]. PREN is defined by the following equation:

$$PREN = wt\%Cr + 3.3((wt\%Mo) + 0.5(wt\%W)) + 16(\text{wt\%N}) \quad (8)$$

The PREN values for the dental alloys under investigation are shown in Table 4. Pitting corrosion resistance is increased with a PREN value of 38. Thus, the three samples were pitting corrosion resistant.

3.2.3. Electrochemical impedance spectroscopy

The Bode and Nyquist curves at −400 mV vs SCE are presented in Fig. 5 (a, b), at −200 mV vs SCE in Fig. 5 (c, d) and at +400 mV vs SCE in Fig. 5 (e, f). The results from the fits to the relevant equivalents circuits models, the theoretical spectra, appear as lines, while the experimental measurements are shown as individual points.

Using Bode plots, the curves of the logarithm of the impedance modulus and the phase shift angle, were plotted as a function of the logarithm of the frequency of the CoCr, C and L samples immersed in Ringer's electrolyte. Fig. 5 (a, c, e) and Table 5 show higher values for the lowest frequency for all three samples, with lower values for sample C and slightly higher values for sample L, indicating a slight increase in the corrosion behavior of the latter alloy, probably caused by Cr addition. Moreover, a specific behavior of the growth of a passive film can be observed for both alloys, which tends to present a capacitive behavior. In general, by applying a more positive potential, the higher the phase angle and impedance values. Consequently, it was observed that the

Table 4
PREN values of the three Co–Cr alloys.

Samples	PREN
CoCr	46.1
L	51.8
C	44.3

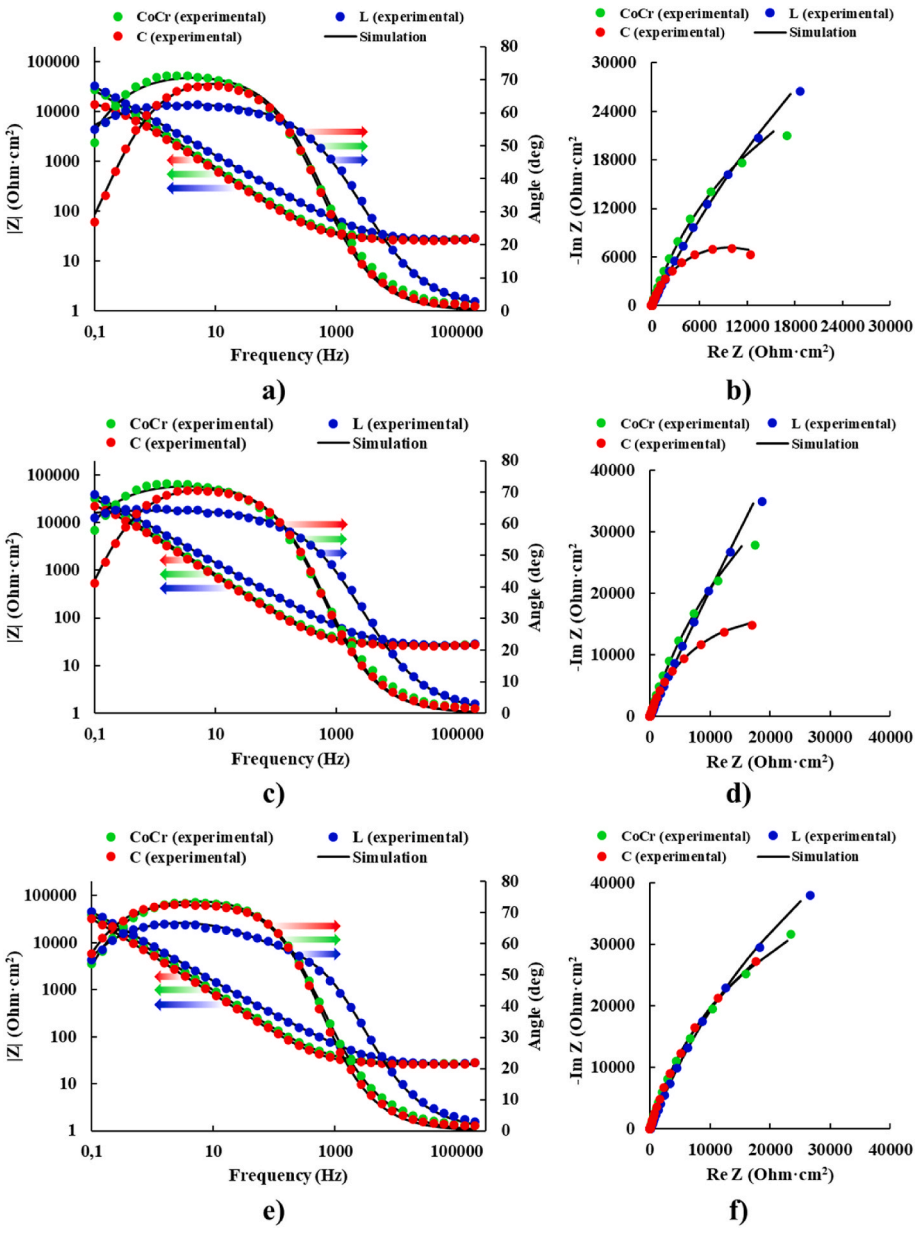

Fig. 5. Bode and Nyquist diagrams of the measured and calculated impedance and angle of the three samples at −0.400 V (a, b) and −0.200 V (c, d) using the equivalent circuit R(QR), and three samples at 0.200 V (e, f) using the equivalent circuit R(Q(R(QR))).

Table 5
Results obtained in the Bode diagrams of the samples studied.

Alloys	Potential (V)	Max. Impedance (Ω)	Max. phase angle (°)
CoCr	−0.400	$2.92{\cdot}10^4$	71
L		$3.48{\cdot}10^4$	63
C		$1.50{\cdot}10^4$	68
CoCr	−0.200	$3.55{\cdot}10^4$	73
L		$4.25{\cdot}10^4$	65
C		$2.41{\cdot}10^4$	71
CoCr	0.400	$4.26{\cdot}10^4$	73
L		$4.98{\cdot}10^4$	66
C		$3.47{\cdot}10^4$	73

Bode phase curves indicated a single phase processes when investigating the three samples. Futrthermore, the phase angle tended to increase with increasing potential value.

In the case of the Nyquist plots, the imaginary impedance values were plotted against the real values. Fig. 5 (b, d, f) showing in all cases a capacitive arc. It can be observed that the L sample presents the highest impedance, a little smaller for CoCr and then the lower value vas obtained for the C sample.

At −400 mV and −200 mV vs SCE the experimental results were fitted with the simple circuit (R(QR)) presented in Fig. 6 while the passive film structure is modified with the potential increasing in such a way that at +400 mV vs SCE the equivalent circuit for these data is more complex (R(Q(R(QR)))) and is presented in Fig. 7.

The simplest equivalent circuit, shown in Fig. 6, allows to fit the experimental data when only charge transfer is taken into consideration. The simple circuit was used to fit the experimental data collected at negative potentials and, in this situation, the theoretical transfer function, Z(ω), is expressed by a parallel combination of a resistor R_1 and a constant phase element Q_1, both in series with the electrolyte resistance R_{sol}.

The experimental data were fitted with the electrical equivalent circuit presented in Fig. 7. R_{sol} corresponds to the electrolyte resistance, the value of which can be estimated by sweeping at high frequencies. R_2

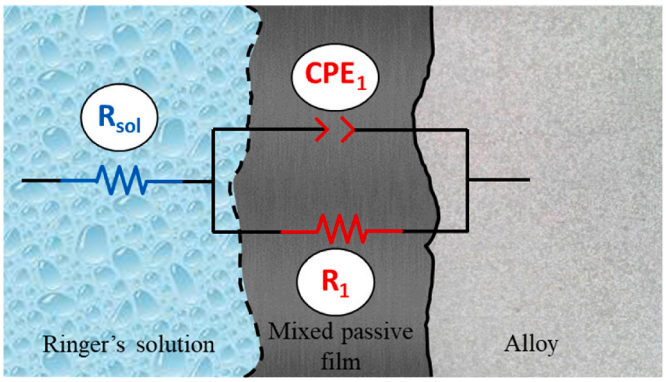

Fig. 6. Equivalent circuit R(QR) to fit the impedance data at −0.400 V and −0.200 V.

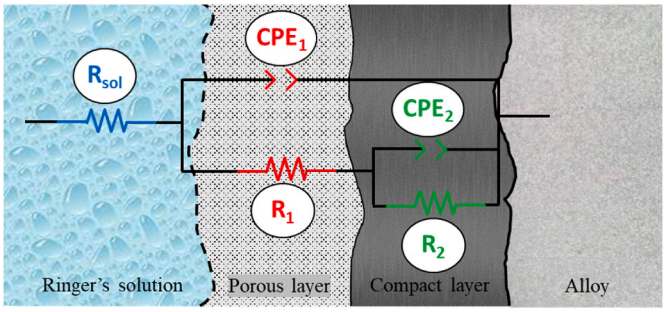

Fig. 7. Equivalent circuit R(Q(R(QR))) to fit the impedance data at 0.400 V.

is the equivalent of the charge transfer resistance, R_{ct}. The capacitance of the double layer C_{dl} (Q_1) is linked to the interactions which take place at the interface between the electrode and electrolyte. A constant phase element (CPE) has been chosen instead of an ideal capacitance [55] in order to be able to take into consideration the heterogeneities of the passive film developed on the metallic surface.

The impedance of a CPE is given by Boukamp (1986) [56]:

$$Z = (j\omega)^{-n} Y^0 \tag{9}$$

Where: (i) j is an imaginary number ($j^2 = -1$); (ii) ω is the angular frequency (rad-s-1); Y_o is the constant of the CPE [$S(s{\cdot}rad^{-1})^n$]; (iv) n is the power number denoting the drift from ideal performance, $n = \alpha(\pi/2)$ and (v) α is the constant phase angle of the CPE (rad).

When fitting the spectrum one of the obtained parameters is the ideality coefficient "n". Therefore, the replica of the real system becomes closer to the ideal one as the value of n approaches unity and as a consequence the surface is more homogeneous. As a result, for n = 1, the CPE element becomes a capacitor with a capacitance Y^0 and for n = 0 just a simple resistor.

The fitting results of the experimental data obtained at negative potentials are presented in Table 6. The polarization resistance (R_2) which takes place at the interface between the metal and the passive film represents the corrosion resistance of the tested metallic sample. It is showed that for the CoCr and C samples the corrosion resistance of R_2 increases as the potential increases since their thickness also increases (Y^0 decreases) and, thus, it can be observed that R_2 increases with increasing Cr content.

For potentials above the corrosion potential, this simple circuit presents unsatisfactory adjustment errors, therefore considering the structural evolution of the passive layer already formed on the surface of the materials a circuit with two time constants has been used. In this way, the existence of differences in the electrochemical behavior of the material function of applied potential or the composition of the material can be revealed.

The equivalent circuit that best fits the experimental data is presented in Fig. 7 and the parameters obtained from EIS data fitting are presented in Table 7.

The component elements are: (i) R_{sol} represents the dissolution resistance; (ii) CPE_1 is the constant phase element corresponding to the porous external passive layer; (iii) R_1 represents the resistance of the external porous layer; (iv) CPE_2 is the constant phase element corresponding to the inner passive layer and (v) R_2 represents the polarization resistance (the corrosion resistance).

From Tables 6 and 7 can be observed that the highest corrosion resistance (R1 in Table 6 and R2 in Table 7) belongs to the sample L which also has the highest Cr concentration.

3.3. Three-point bending test

Load-displacement graphs for the three tested samples were plotted from the three-point bending test. In Fig. 8, the graphs for each specimen were represented and the average of measured elastic modulus values of each alloy had been calculated using the applied force (F), the support spacing at which the lower shank of the equipment is positioned for sample placement (L), the deformation (δ) and the moment of inertia (I), as shown in equation (10).

$$E = \frac{F \cdot L^3}{48 \cdot \delta \cdot I} \cdot 10^{-3} \tag{10}$$

In turn, the moment of inertia depends on the thickness and the length of the sample (see equation (11)).

$$I = \frac{w \cdot h^3}{12} \tag{11}$$

Once the elastic modulus was determined, the average value was calculated for the three examined samples, taking into account as well their mean deviation.

The modulus of elasticity for prosthodontic alloy must be high in order for the prosthesis to withstand bending, specifically in metallic-ceramic restoration parts where bending can cause porcelain fracture [31].

In Table 8, the highest mean value of elastic modulus was obtained for the CoCr specimen and the lower value for the C specimen which has a lower concentration of Cr and Mo and has W in its composition. Therefore, the values of Young's modulus obtained from bending test were relatively low compared to other CoCrMo alloys whose modulus of elasticity values range from 210 to 253 GPa [1,57–59].

4. Conclusions

The following conclusions were obtained in this research.

Table 6
Equivalent circuit R(QR) of the three samples applying potentials of −0.400 V and −0.200 V.

Alloy	−0.400 V				−0.200 V			
	R_{sol} (Ω·cm²)	Y_0 (S·sec^n/cm²)	n	R_1 (Ω·cm²)	R_{sol} (Ω·cm²)	Y_0 (S·sec^n/cm²)	n	R_1 (Ω·cm²)
CoCr	27.54	$4.71{\cdot}10^{-5}$	0.81	$8.17{\cdot}10^{4}$	27.54	$4.22{\cdot}10^{-5}$	0.81	$1.44{\cdot}10^{5}$
L	25.77	$3.01{\cdot}10^{-5}$	0.74	$2.93{\cdot}10^{5}$	25.46	$3.57{\cdot}10^{-5}$	0.72	$1.92{\cdot}10^{5}$
C	26.05	$5.38{\cdot}10^{-5}$	0.81	$1.95{\cdot}10^{4}$	26.02	$4.60{\cdot}10^{-5}$	0.82	$4.14{\cdot}10^{4}$

Table 7
Equivalent circuit R(Q(R(QR))) of the three samples when applying a potential of 0.400 V.

0.400 V							
Alloy	R_{sol} ($\Omega \cdot cm^2$)	Y_{01} ($S \cdot sec^n/cm^2$)	n_1	R_1 ($\Omega \cdot cm^2$)	Y_{02} ($S \cdot sec^n/\cdot cm^2$)	n_2	R_2 ($\Omega \cdot cm^2$)
CoCr	26.79	$2.42 \cdot 10^{-5}$	0.84	47.62	$7.79 \cdot 10^{-6}$	0.83	$9.73 \cdot 10^4$
L	25.93	$2.14 \cdot 10^{-5}$	0.77	$1.03 \cdot 10^3$	$6.99 \cdot 10^{-6}$	0.75	$1.86 \cdot 10^5$
C	26.04	$3.65 \cdot 10^{-5}$	0.84	$1.36 \cdot 10^4$	$4.42 \cdot 10^{-6}$	0.80	$8.66 \cdot 10^4$

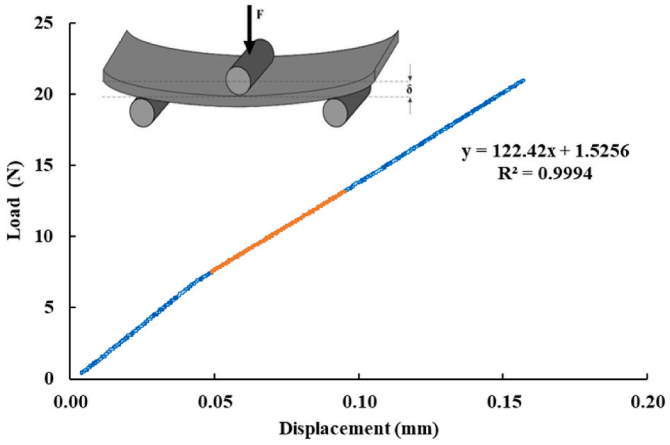

Fig. 8. Three-point flexural test diagram with the experimental arrangement.

Table 8
Modulus of elasticity for the studied alloys.

Sample	E Average (GPa)
CoCr	175 ± 17
C	134 ± 13
L	148 ± 19

- All samples presented a dendritic structure. The samples CoCr and L alloys presented similar microstructure, while the C sample had a slight different structure due to the fact that it had tungsten instead of molybdenum in its composition.
- The samples tend to passivate and have good corrosion resistance, with similar impedance values and higher values for the CoCr and L samples.
- In the three-point bending test, the CoCr and L samples achieved a higher modulus of elasticity than the C specimen. It should also be noted that the modulus of elasticity of this type of alloys (CoCr alloys) is usually between 210 and 253 GPa, so the results obtained are lower than these values.

Therefore, it is possible to confirm the importance of the composition of the samples in their behaviour and properties. The samples CoCr and L, which have the same percentage of molybdenum, show similar results in each test performed, whereas for the sample C, which contains tungsten, is different. Sample C shows a lower corrosion resistance in simulated body fluid and a lower modulus of elasticity, but a higher corrosion potential value. Therefore, the higher Cr content could be the reason for the difference in behaviour between the samples. Based on the results obtained in the previous tests, all the analyzed materials are very adequated for their use in fixed dental prostheses.

Funding

This work was supported by the Romanian National Authority for Scientific Research, CNDI–UEFISCDI, through project number PN-III-P2-2.1-PED-2019-3953, contract 514PED/2020: "New ceramic layer composite material processed by laser techniques for corrosion and high temperature applications—LASCERHEA", within PNCDI III, by Cabildo de Gran Canaria, project number CABINFR2019-07 and by the project ULPGC Excellence, funded by the Department of Economy, Knowledge and Employment of the Canary Islands Government.

CRediT authorship contribution statement

Anca Fratila: Conceptualization, Methodology, Investigation, Writing – original draft, preparation. **Cristina Jiménez-Marcos:** Software, Validation, Investigation, Writing – review & editing. **Julia Claudia Mirza-Rosca:** Conceptualization, Validation, Investigation, Writing – review & editing. **Adriana Saceleanu:** Formal analysis, Resources, Visualization, Supervision.

Declaration of competing interest

The authors declare that they have no known competing financial interests or personal relationships that could have appeared to influence the work reported in this paper.

Data availability

No data was used for the research described in the article.

References

[1] Q. Chen, G.A. Thouas, Metallic implant biomaterials, Mater. Sci. Eng. R Rep. 87 (2015) 1–57, https://doi.org/10.1016/J.MSER.2014.10.001.
[2] K. Prasad, O. Bazaka, M. Chua, M. Rochford, L. Fedrick, J. Spoor, R. Symes, M. Tieppo, C. Collins, A. Cao, D. Markwell, K. Ostrikov, K. Bazaka, Metallic biomaterials: current challenges and opportunities, Materials 10 (2017), https://doi.org/10.3390/MA10080884.
[3] J. Li, X. Liu, Chemical surface modification of metallic biomaterials, Surf. Coat. Modif. Met. Biomater. (2015) 159–183, https://doi.org/10.1016/B978-1-78242-303-4.00005-3.
[4] E.P. Ivanova, K. Bazaka, R.J. Crawford, Cytotoxicity and biocompatibility of metallic biomaterials, New Funct. Biomater. Med. Healthc. (2014) 148–172, https://doi.org/10.1533/9781782422662.148.
[5] S. Kannan, A. Balamurugan, S. Rajeswari, M. Subbaiyan, Metallic implants - an approach for long term applications in bone related defects, Corrosion Rev. 20 (2002) 339–358, https://doi.org/10.1515/CORRREV.2002.20.4-5.339/MACHINEREADABLECITATION/RIS.
[6] A.J. Festas, A. Ramos, J.P. Davim, Medical devices biomaterials – a review, Proc. Inst. Mech. Eng. Part L J. Mater. Des. Appl. 234 (2020) 218–228, https://doi.org/10.1177/1464420719882458/FORMAT/EPUB.
[7] A. Rashidy Ahmady, A. Ekhlasi, A. Nouri, M. Haghbin Nazarpak, P. Gong, A. Solouk, High entropy alloy coatings for biomedical applications: a review, Smart Mater. Manuf. 1 (2023), 100009, https://doi.org/10.1016/j.smmf.2022.100009.
[8] S. Tharani Kumar, S. Prasanna Devi, C. Krithika, R. Raghavan, Review of metallic biomaterials in dental applications, J. Pharm. BioAllied Sci. 12 (2020) 14, https://doi.org/10.4103/jpbs.JPBS_88_20.
[9] V.S. Yadav, M.R. Sankar, L.M. Pandey, Coating of bioactive glass on magnesium alloys to improve its degradation behavior: interfacial aspects, J. Magnesium Alloys 8 (2020) 999–1015, https://doi.org/10.1016/J.JMA.2020.05.005.
[10] C.M. Garcia-Falcon, T. Gil-Lopez, A. Verdu-Vazquez, J.C. Mirza-Rosca, Electrochemical characterization of some cobalt base alloys in Ringer solution, Mater. Chem. Phys. 260 (2021), 124164, https://doi.org/10.1016/J.MATCHEMPHYS.2020.124164.
[11] P.J. Espinoza-Montero, M. Montero-Jiménez, L. Fernández, J.L. Paz, J.L. Piñeiros, S.M. Ceballos, In vitro wearing away of orthodontic brackets and wires in different conditions: a review, Heliyon 8 (2022), e10560, https://doi.org/10.1016/J.HELIYON.2022.E10560.
[12] D.R. Unune, G.R. Brown, G.C. Reilly, Thermal based surface modification techniques for enhancing the corrosion and wear resistance of metallic implants: a

review, Vacuum 203 (2022), 111298, https://doi.org/10.1016/J.VACUUM.2022.111298.
[13] G.L. Turdean, A. Craciun, D. Popa, M. Constantiniuc, Study of electrochemical corrosion of biocompatible Co–Cr and Ni–Cr dental alloys in artificial saliva. Influence of pH of the solution, Mater. Chem. Phys. 233 (2019) 390–398, https://doi.org/10.1016/J.MATCHEMPHYS.2019.05.041.
[14] M. Revilla-León, N.A.H. Husain, M.M. Methani, M. Özcan, Chemical composition, surface roughness, and ceramic bond strength of additively manufactured cobalt-chromium dental alloys, J. Prosthet. Dent 125 (2021) 825–831, https://doi.org/10.1016/J.PROSDENT.2020.03.012.
[15] R. Smeets, B. Stadlinger, F. Schwarz, B. Beck-Broichsitter, O. Jung, C. Precht, F. Kloss, A. Gröbe, M. Heiland, T. Ebker, Impact of dental implant surface modifications on osseointegration, BioMed Res. Int. 2016 (2016), https://doi.org/10.1155/2016/6285620.
[16] M.A. Eskan, G. Uzel, S. Yilmaz, A fixed reconstruction of fully edentulous patients with immediate function using an apically tapered implant design: a retrospective clinical study, Int. J. Implant Dent. 6 (2020), https://doi.org/10.1186/S40729-020-00271-1.
[17] F. Rupp, L. Liang, J. Geis-Gerstorfer, L. Scheideler, F. Hüttig, Surface characteristics of dental implants: a review, Dent. Mater. 34 (2018) 40–57, https://doi.org/10.1016/J.DENTAL.2017.09.007.
[18] C.M. Garcia-Falcon, T. Gil-Lopez, A. Verdu-Vazquez, J.C. Mirza-Rosca, Corrosion behavior in Ringer solution of several commercially used metal alloys, Anti-corrosion Methods & Mater. 68 (2021) 324–330, https://doi.org/10.1108/ACMM-05-2021-2486.
[19] G. Bayramoğlu, T. Alemdaroğlu, S. Kedici, A.A. Aksüt, The effect of pH on the corrosion of dental metal alloys, J. Oral Rehabil. 27 (2000) 563–575, https://doi.org/10.1046/J.1365-2842.2000.00549.X.
[20] D. Pupim, R. Fernandes, A. Paula, R.G. Palma-dibb, Influence of the commercial mouthwashes on the corrosion behaviour of dental alloy, Mater. Res. 25 (2022), https://doi.org/10.1590/1980-5373-MR-2021-0385.
[21] J.C. Hornez, A. Lefèvre, D. Joly, H.F. Hildebrand, Multiple parameter cytotoxicity index on dental alloys and pure metals, Biomol. Eng. 19 (2002) 103–117, https://doi.org/10.1016/S1389-0344(02)00017-5.
[22] Z. Ahmad, Porcelain fused to metal (PFM) crowns and caries in adjacent teeth, J. Coll. Physicians Surg. Pakistan. 21 (2011) 134–137. http://ecommons.aku.edu/pakistan_fhs_mc_surg_dent_oral_maxillofac/11. (Accessed 18 April 2022).
[23] Y. Lu, W. Chen, W. Ke, S. Wu, Nickel-based (Ni–Cr and Ni–Cr–Be) alloys used in dental restorations may be a potential cause for immune-mediated hypersensitivity, Med. Hypotheses 73 (2009) 716–717, https://doi.org/10.1016/J.MEHY.2009.04.041.
[24] G. Alp, G. Çakmak, M. Sert, Y. Burgaz, Corrosion potential in artificial saliva and possible genotoxic and cytotoxic damage in buccal epithelial cells of patients who underwent Ni-Cr based porcelain-fused-to-metal fixed dental prostheses, Mutat. Res. Toxicol. Environ. Mutagen. 827 (2018) 19–26, https://doi.org/10.1016/J.MRGENTOX.2018.01.004.
[25] A.J. Fernandes Neto, H. Panzeri, F.D. Neves, R.A. Do Prado, G. Mendonça, Bond strength of three dental porcelains to Ni-Cr and Co-Cr-Ti alloys, Braz. Dent. J. 17 (2006) 24–28, https://doi.org/10.1590/S0103-64402006000100006.
[26] I.C.M. Moris, M. Sakuma, A.C.L. Faria, A.P. Macedo, R.F. Ribeiro, R.C.S. Rodrigues, The dental alloys determine the choice of composite resins to be used, Brazilian Dent. Sci. 20 (2017) 92–98, https://doi.org/10.14295/BDS.2017.V20I1.1329.
[27] R.L.W. Messer, L.C. Lucas, Evaluations of metabolic activities as biocompatibility tools: a study of individual ions' effects on fibroblasts, Dent. Mater. 15 (1999) 1–6, https://doi.org/10.1016/S0109-5641(99)90023-4.
[28] S.S. Sidhu, H. Singh, M.A. Gepreel, A review on alloy design, biological response, and strengthening of β-titanium alloys as biomaterials, Mater. Sci. Eng. C 121 (2021), 111661, https://doi.org/10.1016/j.msec.2020.111661.
[29] S. Mercieca, M. Caligari Conti, J. Buhagiar, J. Camilleri, Assessment of corrosion resistance of cast cobalt- and nickel-chromium dental alloys in acidic environments, J. Appl. Biomater. Funct. Mater. 16 (2018) 47–54, https://doi.org/10.5301/jabfm.5000383.
[30] J. Qiu, W.Q. Yu, F.Q. Ohang, R.J. Smales, Y.L. Ohang, C.H. Lu, Corrosion behaviour and surface analysis of a Co-Cr and two Ni-Cr dental alloys before and after simulated porcelain firing, Eur. J. Oral Sci. 119 (2011) 93–101, https://doi.org/10.1111/J.1600-0722.2011.00791.X.
[31] J.C. Wataha, Alloys for prosthodontic restorations, J. Prosthet. Dent 87 (2002) 351–363, https://doi.org/10.1067/mpr.2002.123817.
[32] A. Marti, Cobalt-base alloys used in bone surgery, Injury 31 (2000) D18–D21, https://doi.org/10.1016/S0020-1383(00)80018-2.
[33] Y.S. Al Jabbari, Physico-mechanical properties and prosthodontic applications of Co-Cr dental alloys: a review of the literature, J. Adv. Prosthodont. 6 (2014) 138–145, https://doi.org/10.4047/JAP.2014.6.2.138.
[34] T. Hanawa, Overview of metals and applications, Met. Biomed. Devices (2010) 3–24, https://doi.org/10.1533/9781845699246.1.3.
[35] V.V. Kuznetsov, E.A. Filatova, A.V. Telezhkina, S.S. Kruglikov, Corrosion resistance of Co−Cr−W coatings obtained by electrodeposition, J. Solid State Electrochem. 22 (2018) 2267–2276, https://doi.org/10.1007/S10008-018-3929-8/FIGURES/7.
[36] C.M. Garcia-Falcon, T. Gil-Lopez, A. Verdu-Vazquez, J.C. Mirza-Rosca, Analysis and comparison of the corrosive behavior of nickel-based and cobalt-based dental alloys, Mater 14 (2021) 4949, https://doi.org/10.3390/MA14174949, 14 (2021) 4949.
[37] M.C. Conti, A. Karl, P.S. Wismayer, J. Buhagiar, Biocompatibility and characterization of a Kolsterised ® medical grade cobalt-chromium-molybdenum alloy, Biomatter 4 (2014), e27713, https://doi.org/10.4161/biom.27713.
[38] A. Mahajan, S.S. Sidhu, S. Devgan, MRR and surface morphological analysis of electrical-discharge-machined Co–Cr alloy, Emerg. Mater. Res. 9 (2020) 1–5, https://doi.org/10.1680/jemmr.19.00034.
[39] S. Viennot, F. Dalard, M. Lissac, B. Grosgogeat, Corrosion resistance of cobalt-chromium and palladium-silver alloys used in fixed prosthetic restorations, Eur. J. Oral Sci. 113 (2005) 90–95, https://doi.org/10.1111/J.1600-0722.2005.00190.X.
[40] S.E.P. Gonçalves, E. Bresciani, Reconstructions using alloys and ceramics, Mater. Interfacial Phenom. Contrib. from Dent. Craniofacial Reconstr. (2017) 23–66, https://doi.org/10.1016/B978-0-08-100330-5.00002-9.
[41] R.M. Carranza, M.A. Rodríguez, Crevice corrosion of nickel-based alloys considered as engineering barriers of geological repositories, Npj Mater. Degrad. 11 (1) (2017) 1–9, https://doi.org/10.1038/s41529-017-0010-5 (2017).
[42] S.R.M.M. De Aguiar, M. Nicolai, M. Almeida, A. Gomes, Electrochemical behaviour of a cobalt–chromium–molybdenum dental alloy in artificial salivas, Bio Med. Mater. Eng. 25 (2015) 53–66, https://doi.org/10.3233/BME-141241.
[43] A. Vaicelyte, C. Janssen, M. Le Borgne, B. Grosgogeat, Cobalt–chromium dental alloys: metal exposures, toxicological risks, CMR classification, and EU regulatory framework, Crystals 10 (2020) 1151, https://doi.org/10.3390/cryst10121151.
[44] H.A. Zaman, S. Sharif, D.-W. Kim, M.H. Idris, M.A. Suhaimi, Z. Tumurkhuyag, Machinability of cobalt-based and cobalt chromium molybdenum alloys - a review, Procedia Manuf. 11 (2017) 563–570, https://doi.org/10.1016/j.promfg.2017.07.150.
[45] A. Mahajan, S. Devgan, S.S. Sidhu, Surface alteration of biomedical alloys by electrical discharge treatment for enhancing the electrochemical corrosion, tribological and biological performances, Surf. Coating. Technol. 405 (2021), 126583, https://doi.org/10.1016/j.surfcoat.2020.126583.
[46] P. Sahoo, S.K. Das, J. Paulo Davim, Tribology of materials for biomedical applications, Mech. Behav. Biomater. (2019) 1–45, https://doi.org/10.1016/B978-0-08-102174-3.00001-2.
[47] J. Radwan-Pragłowska, Ł. Janus, E. Szajna, T. Galek, A. Sierakowska, M. Piątkowski, M. Tupaj, P. Radomski, M. Michalec, D. Bogdał, Biodegradable Mg-based implants obtained via anodic oxidation applicable in dentistry: preparation and characterization, J. Mater. Res. Technol. 20 (2022) 1736–1754, https://doi.org/10.1016/J.JMRT.2022.07.064.
[48] A.K. Mishra, D.W. Shoesmith, Effect of alloying elements on crevice corrosion inhibition of nickel-chromium-molybdenum-tungsten alloys under aggressive conditions: an electrochemical study, Corrosion 70 (2014) 721–730, https://doi.org/10.5006/1170.
[49] A. Łukaszczyk, J. Augustyn-Pieniązek, Corrosion resistance of Co-Cr-Mo alloy used in dentistry, Arch. Metall. Mater. 60 (2015) 523–528, https://doi.org/10.1515/amm-2015-0084.
[50] J.V. Giacchi, C.N. Morando, O. Fornaro, H.A. Palacio, Microstructural characterization of as-cast biocompatible Co-Cr-Mo alloys, Mater. Char. 62 (2011) 53–61, https://doi.org/10.1016/j.matchar.2010.10.011.
[51] M. Pourbaix, H. Zhang, A. Pourbaix, Presentation of an atlas of chemical and electrochemical equilibria in the precence of a gaseous phase, Mater. Sci. Forum 251–254 (1997) 143–148. https://doi.org/10.4028/www.scientific.net/MSF.251-254.143.
[52] X. Wang, W. qing Qin, F. Jiao, L. yang Dong, J. gen Guo, J. Zhang, C. ren Yang, Review of tungsten resource reserves, tungsten concentrate production and tungsten beneficiation technology in China, Trans. Nonferrous Metals Soc. China 32 (2022) 2318–2338, https://doi.org/10.1016/S1003-6326(22)65950-8.
[53] B. Chen, Z.B. Li, J.R. Liu, G.H. Zhang, Effect of molybdenum addition on microstructure and mechanical properties of 90% tungsten heavy alloys, Int. J. Refract. Met. Hard Mater. 106 (2022), 105868, https://doi.org/10.1016/J.IJRMHM.2022.105868.
[54] S. Papavinasam, Modeling – internal corrosion, Corros. Control Oil Gas Ind (2014) 301–360, https://doi.org/10.1016/B978-0-12-397022-0.00006-6.
[55] N. Ibriş, J.C. Mirza Rosca, EIS study of Ti and its alloys in biological media, J. Electroanal. Chem. 526 (2002) 53–62, https://doi.org/10.1016/S0022-0728(02)00814-8.
[56] B.A. Boukamp, A Nonlinear Least Squares Fit procedure for analysis of immittance data of electrochemical systems, Solid State Ionics 20 (1986) 31–44, https://doi.org/10.1016/0167-2738(86)90031-7.
[57] T.G. de Oliveira, D.V. Fagundes, P. Capellato, D. Sachs, A.A.A.P. da Silva, A review of biomaterials based on high-entropy alloys, Metals 12 (2022) 1940, https://doi.org/10.3390/met12111940.
[58] M. Long, H.J. Rack, Titanium alloys in total joint replacement - a materials science perspective, Biomaterials 19 (1998) 1621–1639, https://doi.org/10.1016/S0142-9612(97)00146-4.
[59] M. Ogawa, Y. Tohma, H. Ohgushi, Y. Takakura, Y. Tanaka, Early fixation of cobalt-chromium based alloy surgical implants to bone using a tissue-engineering approach, Int. J. Mol. Sci. 13 (2012) 5528, https://doi.org/10.3390/IJMS13055528.